Latent heat flux sensitivity to sea surface temperature – regional perspectives

B. Praveen Kumar[1] , Meghan F. Cronin[2], Sudheer Joseph[1], M. Ravichandran[1] and N. Sureshkumar[1]

1. *ESSO Indian National Centre for Ocean Information Services (INCOIS), Hyderabad, India*
2. *NOAA Pacific Marine Environmental Laboratory (PMEL), Seattle, WA, USA*

Revised for Journal of Climate

11/26/16

Corresponding Author Address:

B. Praveen Kumar

Modelling and Ocean Observations Group

Indian National Centre for Ocean Information Services (INCOIS)

Hyderabad,Telangana State

India – 500090

E-mail: praveen.b@incois.gov.in

Abstract

A global analysis of Latent Heat Flux (LHF) sensitivity to Sea Surface Temperature (SST) is performed, with focus on the tropics and the North Indian Ocean (NIO). Sensitivity of LHF state variables (wind speed (W_s) and vertical humidity gradients (Δq)) to SST give rise to mutually interacting dynamical (W_s-driven) and thermodynamical (Δq-driven) coupled feedbacks. Generally, LHF sensitivity to SST is pronounced over tropics where SST increase causes W_s (Δq) changes, resulting in a maximum decrease (increase) of LHF by ~15W/m^2/°C. But Bay of Bengal (BoB) and Northern Arabian Sea (NAS) remain an exception that is opposite to the global feedback relationship. This uniqueness is attributed to strong seasonality in monsoon W_s and Δq variations which brings in warm (cold) continental airmass into BoB and NAS during summer (winter), producing large seasonal cycle in air-sea temperature difference (ΔT, and hence on Δq). In other tropical oceans, surface air is mostly of marine origin and blows from colder to warmer waters, resulting in a constant ΔT~1°C throughout the year, and hence a constant Δq. Thus unlike other basins, when BoB and NAS are warming, air temperature warms faster than SST. The resultant decrease in ΔT and Δq contributes to decrease the LHF with increased SST, contrary to other basins. Our analysis suggests that in NIO, LHF variability is largely controlled by thermodynamic processes, which peak during the monsoon period. These observed LHF sensitivities are then used to speculate how the surface energetics and coupled feedbacks may change in a warmer world.

Key words: Latent Heat Flux, Dynamic and thermodynamic contributions, North Indian Ocean, Monsoon winds

1. Introduction

Air-Sea heat fluxes are important components of the climate system, through which the ocean and atmosphere exchange energy and keep the earth system in a '*balanced*' climate state. Latent Heat Flux (LHF), the second largest term in the flux budget (second only to surface solar radiation), is the heat used to evaporate water from the ocean surface, resulting in ocean cooling, which is then released to warm the atmosphere when the vapor condenses to form clouds (Taylor 2003). LHF plays a central role in coupling the atmosphere and the ocean. This coupling involves both dynamical (e.g., the Bjerknes feedback) and thermodynamical (e.g., flux-SST feedback) feedbacks between the ocean and atmosphere.

Traditionally LHF is estimated following a bulk formula (Fairall et al. 1996, 2003) that is a function of surface wind speed (W_s), air-sea humidity gradient (Δq) and a transfer coefficient (C_h). But this direct proportionality of W_s and vertical Δq with LHF in the bulk formula is often deceptive since the transfer coefficient can change with W_s, and to a certain extent with Sea Surface Temperature (SST). Likewise, an increase in wind speed can result in increased latent and sensible heat loss from the ocean, reducing the SST, and thus reducing the vertical humidity gradient. As a consequence, the relation between LHF and W_s versus vertical Δq can differ for the same unit SST change in different basins. The sensitivity of LHF to SST has been studied in the past, but most of such investigations were restricted to the tropical Pacific (see Zhang and McPhaden 1995 and the references therein). These problems underscore the need to better understand the distribution of LHF variability over the world oceans, and in particular, it's controlling dynamic (i.e., driven by wind) and thermodynamic (i.e., driven by humidity gradient) components.

Understanding the role of thermodynamic processes in controlling LHF variation with changes in SST through the vertical Δq is relatively straightforward: surface saturation vapor pressure increases exponentially with increase in SST as per the Clausius-Clapeyron relation, correspondingly increasing the vertical Δq. However, wind speed variation with respect to SST is complicated, and hence the role of dynamic processes in controlling LHF variation is difficult to understand. Ramanathan and Collins (1992), using moist static energy analysis of the surface air, showed that the surface air is convectively unstable at high SST (> 300°K). Those convectively unstable areas are subject to low-level convergence, with low wind speed at the center of convergence, limiting the LHF (Neelin and Held 1987; Liu 1988). Thus at high SSTs, dynamic processes dominates LHF. Sui et al (1991) using a coupled atmosphere-ocean boundary layer model, showed that the LHF characteristics can change significantly with or without the coupling between atmospheric and oceanic boundary layer. In their experiments, when both the SST and the surface winds are prescribed (i.e., no interaction between the SST and the surface wind is allowed), LHF is found to increase with SST due to the increase of humidity difference.

Questions on the limiting role of SST on flux exchanges have been investigated in many past studies (Frankignoul and Hasselmann 1977, Wallace 1992, Zhang et al. 1995, Zhang and McPhaden 1995, Barsugli and Battisti 1998, Wu et al. 2006, 2007, Gao et al. 2013, Nisha et al. 2014). Using moored buoy data from the equatorial Pacific, Zhang and McPhaden (1995, hereinafter ZM95) studied the relationship between LHF and SST and found that there is a threshold SST of 301°K, above and below which the relationship of LHF with SST is contrasting. At low (high) SST, LHF increases (decreases) with SST - a relationship that can't be explained by thermodynamic considerations alone. Analysis of the wind speeds and surface humidity gradients indicated that at low SST, the vertical humidity difference primarily determines the LHF, and at

high SST a sharp decrease in wind speed is mostly responsible for the low LHF. They have further shown that the low LHF at high SST is because of the complex interaction between convection and large scale circulation in the equatorial Pacific. Nisha et al (2014) using similar methodology, reached analogous conclusions in NIO. These results suggest that the contrasting behavior of the dynamic and thermodynamic processes of LHF at different ranges of SST, indeed, help to maintain an equilibrium temperature of the ocean. Gao et al (2013) studied the global changes in LHF and found that ~70% of the total temporal variations in LHF are contributed by Δq changes while the rest are contributed by wind variations. They further noted that the change in Δq is due both to increase in sea surface saturation humidity (q_s) and decrease in air humidity (q_a), and contribution of q_s is nearly three times as much as that of q_a.

Seager et al (2003) and Sobel (2003) looked at the SST-flux feedback in the context of global energetics. Sobel (2003) suggested that the deep convective clouds over the warm pool reduce the amount of surface solar radiation that the LHF has to balance. Weaker (stronger) wind speeds over the equatorial warm pool (off equatorial) regions reduce (increase) the LHF and increase (decrease) the SST. Consequently, the wind speed distribution increases the meridional temperature gradient and increases the poleward ocean heat transport. Low (high) LHF over the warm pool (under trade winds) can be sustained because the incoming solar radiation is partially offset by ocean heat flux divergence (convergence) (Sobel. 2003, Dinezio et al. 2009). Seager et al (2003) has shown that under the trade winds, advection of moisture in the atmospheric boundary layer from the subtropics to the equator increases the evaporation provided oceanic heat transport exists locally, but this has a smaller effect than the wind speed or the cloud -radiation interactions. One of the central themes of these results is the way in which SST and fluxes interact with each other. Understanding the role of SST on LHF through its dynamic and

thermodynamic effects is hence an important pre-requisite for answering how Earth maintains the climate through energy transport and what its perceived changes are.

Research into the air-sea flux - SST relation in the Indian Ocean has lagged that in the rest of the tropical oceans owing mainly to the scarcity of good quality data, and partially to the notion that relations from tropical Pacific applies elsewhere. This trend took a positive turnaround with the focused and well-coordinated research experiments in the tropical Indian Ocean during the Bay of Bengal Monsoon Experiment (Bhat et al. 2001b) and Arabian Sea Monsoon Experiment (Sengupta et al. 2008). One of the major outcomes of these experiments was the identification of the unique nature of the lower boundary layer conditions in the tropical Indian Ocean. Bhat (2001a), using data from BOBMEX experiment concluded that the air-sea temperature gradient in the Bay of Bengal during boreal summer is very close to zero and can even reverse during the diurnal cycle. This is unlike any other tropical basins, and paves the way for a focused investigation into the implications of such a small air-sea temperature gradient on flux exchanges. But to date, the effects of the small air-sea temperature gradient or the strong seasonality observed in the tropical Indian Ocean on the large scale flux exchanges are not well studied. Implications of this particular feature will be addressed explicitly in this article.

Unlike ZM95 or Nisha et al (2014) which were focused on finding a threshold SST at which both dynamic and thermodynamic processes of LHF balance, the present study aims to identify and understand how the dynamic and thermodynamic processes differ over an SST range in different basins. The rest of the paper is organized as follows: Section two describes the data used and the methodology followed in this study. Our main findings are described in section 3. In section 4, we conclude with a summary of results and a discussion of how these

observed LHF sensitivities to SST may provide a clue to how the surface energy balance may change in a warmer world.

2. Data and Methods

In this section, first we briefly describe the various data sets used in this study. This is then followed by the basic methodology we used to separate the wind and humidity contributions to the total LHF variability through their dependence upon SST variations.

2.1. Data

We used daily gridded data sets from Objectively Analyzed air-sea Fluxes project (OAFlux) for most of the analyses in this paper (Yu et al. 2007). OAFlux project utilizes various sources of meteorological variables, and develops a blended product following an objective analysis (Yu et al. 2007). Objective analysis reduces error in each input data source and produces an estimate that has the minimum error variance. The OAFlux project uses the objective analysis to obtain optimal estimates of flux-related surface meteorology and then computes the global fluxes by using the state-of-the-art bulk flux parameterizations.

In addition to the blended products described above, additional data sets for wind and air temperature (T_a) at different pressure levels in the atmosphere are obtained from the National Centers for Environmental Prediction / National Center for Atmospheric Research (NCEP/NCAR) reanalysis (Kalney et al. 1996). For all analyses, we use the same period, from 1985 to 2013.

2.2 Methodology

Latent heat flux (LHF) can be conveniently estimated following the traditional bulk formula as follows:

$$LHF = \rho L_v C_h W_s . \Delta q, \quad (1)$$

where ρ is the air density (1kg/m^3), L_v is the latent heat of vaporization (2.44 x10^6 J/kg), C_h is the transfer coefficient (1.3 x 10^{-3}), W_s is the 10 m wind speed and $\Delta q = (q_s - q_{2m})$ is the humidity gradient between sea surface and the air 2 m above it. Saturation humidity (q_s) at the sea surface is calculated using SST. The transfer coefficient variation is relatively constant ($C_h \approx 1.3 \times 10^{-3}$), but has some variation associated with wind speed and the stability of the air column, which is directly related to the vertical humidity gradient. Neglecting the effects of the transfer coefficient, the relative contribution of wind and humidity gradient to the LHF feedback can be determined by differentiating equation (1) with respect to SST as follows (See Zhang and McPhaden. 1995):

$$\frac{d(LHF)}{d(SST)} = \rho L_v C_h \left[\frac{dU}{dSST}(q_s - q_{2m})\right] + \rho\, L_v C_h \left[U \frac{d(q_s - q_{2m})}{dSST}\right] \qquad (2)$$

This feedback equation (2) is evaluated at every grid point using daily OAFlux data. Each calculation requires data from two adjacent days and was done 10591 times at each grid point from 1 January 1985 to 31 December 2013. Coincident changes with SST are computed grid-wise by estimating least square regression of the differential terms and then multiplying with the daily variables as shown in equation (2). The statistical significance of this calculation is analyzed based on the significance of the least square regression at each grid point. Here, the first term on the right explains the wind (i.e., dynamic) contribution to the LHF variability associated with a unit SST change and the second term explains the humidity (i.e., thermodynamic) contribution on LHF variability associated with the unit SST change. Also note that we defined LHF as a positive quantity such that a positive (negative) value for LHF anomaly indicates an increase (decrease) in LHF loss from the ocean.

It is to be noted that instead of using the LHF provided by the OAFlux product, we computed LHF using daily mean values of W_s and Δq from OAFlux, and constant values of ocean heat capacity and transfer constant. Flux calculated this way have mean offsets with respect to the gridded flux provided by the OAFlux product, sometimes as high as 50%, although the variability matches well (Alexander and Scott, 1997). This can be due, in part, to the choice of the bulk formula and the way variables are stored and averaged. Within the tropical belt, the root mean square difference between our computed LHF and the OAFlux provided LHF is ~40W/m^2. This difference is higher in regions of strong warm currents such as Gulf Stream, Kuroshio, Agulhas, Lewin, east Australian currents etc, where it can reach upto 80W/m^2.

3. Results

Figure 1 shows the mean coincident variation of LHF with unit change in SST at each grid point and its dynamical and thermodynamical components. Figure 1a suggests that generally along the equator and in the eastern portion of most basins, there is a net increase of LHF with increased SST. At other locations a net decrease of LHF with increased SST is observed. Once the total LHF variation with SST is separated into its wind and humidity contributions, most of the global oceans behave uniformly, i.e., coincident wind variation with increased SST tends to suppress the LHF, and coincident humidity gradient changes with increased SST tends to increase the LHF. The dynamical (i.e., associated with wind variations) and thermodynamical (i.e., associated with humidity changes) contributions on LHF are stronger in the tropical warm oceans with SST above ~25°C where it can be as high as 15W/m^2 for every degree change in SST. But at each location, either of these processes dominate, and the dominant process regulate the LHF variability as a function of SST (figure 1a). In this context, Bay of Bengal (BoB) and North Arabian Sea (NAS), the two North Indian Ocean (NIO) basins

stand-out in figure 1b and 1c because of their contrasting behavior compared to other parts of the world oceans. This indicates that though the LHF variations with respect to SST in NIO are somewhat similar to other basins (figure 1a), their contributing factors are clearly different (figure 1b and 1c).

One important characteristic of NIO is its land-locked northern boundary and strong seasonality (Schott et al. 2009). But there are other basins where similar characteristics are prevailing but not showing any uniqueness as far as the control of wind and air-sea humidity gradient on LHF is concerned. For example, Gulf of Mexico and Caribbean Sea between North and South America fall almost in the same latitudinal bands as NIO, which are also land-locked, but no noticeable aspects are found in figures 1b and 1c. Similarly, extra-tropical oceans have strong annual cycle, primarily owing to the seasonal migration of sun, but still follow the general global trend seen in figures 1b and 1c. This is an incentive to focus more on the NIO to find out what exactly causes the uniqueness seen in figure 1. In the following sections, we provide general discussions and explanations for LHF variability in the world oceans, with a particular focus on the two NIO basins.

3.1 LHF variability with respect to SST

Figure 2 shows the variation of LHF and its controlling variables as a function of SST. In the global tropical oceans (we define 30°S-30°N band as tropical oceans), the humidity gradient is relatively uniform (~4g/kg) below an approximate 25°C SST threshold; above this threshold, it increases sharply with increase in SST (at a rate of 1g/kg/°C; see figure 2a). This exponential relation is in accordance with the Clausius-Clapeyron relation, and results in a sharp increase of LHF with SST in the warmer waters (SST > 25°C). Overall in the global tropics, wind speed

varies little with respect to SST below ~25°C; above this threshold, however, it decreases with further increase in SST (at a rate of ~1m/s/°C). The slopes of various curves in figure 2c indicate the corresponding value of LHF variations associated with that SST range. These observations are consistent with that of Ramanathan and Collins (1992) that the warm waters help form a low-level convergence in the lower boundary layer, with weak wind speed at the center of convergence, resulting in a decrease of LHF over the warm waters. These opposing dynamic (W_s) and thermodynamic (Δq) effects result in a relatively weak change in LHF for a 1°C SST change across the full range of SST averaged in the tropical oceans (see the thick line in figure 2c).

As shown in figure 1, BoB and NAS exhibit unique characteristics compared to the other tropical basins, especially in the 25-28°C SST range, but follow the general global patterns above ~28°C (Figure 2). Humidity gradient in the two NIO basins decreases sharply in the 25-28°C SST range. Similarly wind speed picks up in 25-28°C range whereas in other tropical basins it slows down with SST. Figure 2c suggests that LHF variability in the NIO is similar and comparable to the tropical basins averaged values even in the 25-28°C SST range, but it can be inferred from figures 2a, and 2b that its contributing factors are clearly different.

The unique features observed in the two NIO basins (BoB and NAS) are an incentive to focus on the two basins in the coming sections. Figure 3 shows how Δq, W_s and LHF vary with respect to SST in different seasons in NIO. The Δq, W_s and LHF variability in the <25°C range are mostly controlled by DJF values, and in warm SST range, MAM values control the variability. It is remarkable that for the same SST range of 25-28°C, NAS (BoB) exhibits a Δq difference of ~ 5g/kg (~3.5g/kg) and wind speed difference of ~ 4m/s between winter and summer, indicative of the large seasonal cycle of these basins (figure 3a-d). Seasonal variation of LHF for the same SST

range can be as large as 50W/m^2 in NAS and 35W/m^2 in BoB (figures 3e and 3f). A closer look at these figures further suggests that, in general, Δq increases with SST in most of the seasons in both basins except during SON and DJF in the BoB in the 25-28°C SST range. Similarly, in both basins, yearly-averaged W_s increases with increased SST in the colder SST range but decreases with increased SST in the warmer SST range (full lines in figures 3c and 3d). In NAS, the JJA and SON mean W_s decrease with SST increase starts at relatively low temperatures (24-25°C). These observations are in general agreement with that of ZM95 from the tropical Pacific (see their figures 6, 7 and 8). But the wide seasonal range of Δq and W_s with SST in the NIO basins makes the annual cycle of these controlling variables behave differently with respect to SST compared to other basins.

The discussions so far indicate that the large seasonal cycle in the NIO basins (Figure 3) might be the reason for the kind of uniqueness observed in figures 1 and 2. If that is true, then why don't other similar basins with land locked topography and/or with large seasonal cycles in the LHF controlling variables show a similar kind of behavior as the NIO basins? This question is explicitly answered in the next sections.

3.2 Unique Air-Sea Temperature Variations in the North Indian Ocean

Discussions in the previous section suggest that wind and humidity variations that are coincident with SST changes in the NIO differ from other tropical basins in the 25-28°C SST range, although above that threshold the NIO follows the global pattern. Both BoB and NAS are warm basins where the climatological SST is generally above 24°C in most of the seasons (de Boyer et al. 2007) and throughout much of the year it is in the 25-28°C range. Hence in the next

sections, we focus on the 25-28°C SST range to understand the uniqueness of processes leading to the LHF variability in the NIO basins.

Figure 4a show the sea-air temperature gradient (ΔT) in the tropical oceans in the 25-28°C SST range. It is important to realize that these represent different periods and lengths of time, in different regions. However focusing on this temperature range helps to diagnose the thermodynamic feedback mechanism. In general, SST is always warmer than the air just above the sea surface in the tropical oceans. Throughout most of the tropical oceans, a coincident change of ΔT with a unit change in SST is generally positive (figure 4b), implying that the SST warms faster than the air above it. In NIO, South China Sea and Gulf of Mexico, however, the rate of change in ΔT with a unit change in SST is negative (see figure 4b), implying that air warms at a faster rate than SST in these locations. This suggests that for the same SST range, unlike in the rest of the tropical oceans, NIO basins support warmer T_a and hence the surface air can hold more moisture. Figure 4c shows the rate of change of saturation specific humidity of air with SST in the 25-28°C SST range. Saturation specific humidity (q_s) is the capacity of air to hold the maximum amount of humidity, and hence is a proxy for the water holding capacity of air. Since q_s is a function of temperature and increases nearly exponentially with temperature, in the 25-28°C SST range, T_a is higher in the NIO compared to other basins and thus the water holding capacity of air increases much faster there (figure 4c). It is clear that among the tropical oceans, NIO shows the maximum increase in saturation humidity with SST changes and hence in that SST range the sea-air humidity gradient will be minimum in NIO. This indicates that while ocean processes control the positive thermodynamic SST-LHF feedback throughout much of the tropical ocean, other processes play a role in driving a negative thermodynamic feedback in the NIO. That is, in the

NIO, we hypothesize that the influence of nearby land causes the T_a to increase faster than SST, resulting in a weak vertical humidity gradient that reduces the latent flux loss with increased SST.

The large scale wind patterns over the tropical oceans, which advect warm / cold air from other locations, play a crucial role in controlling T_a. Figure 5 shows the large scale wind patterns and T_a averaged over 1000-850mb heights (which is roughly average over 1.5 km range from the earth/ocean surface). NIO is characterized by the unique seasonal reversal of the wind patterns, which is south-westerly during summer and north-easterly during winter. In the peak of winter, i.e., during DJF, the land temperatures over much of Asian landmass is cooler than that of the surrounding oceans. The prevailing north-easterly winds bring in this cold air mass into the two NIO basins and reduces the T_a there. So once the winter season starts, the air temperature over NIO basins starts to decrease rapidly. During the peak of summer, the winds are mostly south-westerlies over NIO, and the land air is very warm compared to the ocean temperatures. A closer look at figure 5c suggests that large scale wind patterns over BoB is mostly coming from the Indian land mass, which brings in warm air into the Bay. Similarly, the southward winds over the very warm Arabian Peninsula feeds the northern part of the Arabian Sea with hot air. The net effect is that during summer, T_a over the BoB and NAS basins warms faster than that of SST. Note that this effect in Arabian Sea is mostly restricted to the northern part of the basin, whereas the land effect over the Bay of Bengal is mostly over the entire basin (See Appendix).

Thus during summer, the large scale winds over BoB and NAS bring warm air from Indian subcontinent and Arabian Peninsula into the ocean. This, together with fact that the summer SST in those basins is also much warmer, help to maintain a small ΔT. During winter, large scale wind pattern over these basins brings much colder air from the land into the oceans. The resulting cold air intrusion on the lower layers of the boundary layer makes it cold and dense,

resulting in a large ΔT near the ocean surface. Thus the monsoonal reversal of wind pattern produces a sharp decrease of T_a during SONDJF (September-to-February) and a sharp increase during MAMJJA (March-to-August). Consequently, the annual cycle of T_a in BoB and NAS is stronger than that of SST, producing a very pronounced annual cycle in ΔT.

Over most of tropical Pacific and Atlantic, winds are always of maritime origin. The large scale winds blow from regions of cool SST towards warm SST, and hence the surface air is moist and cooler than the SST. This results in maintaining a large, constant ΔT throughout the year, hence resulting in nearly constant Δq year-round. It is interesting to note that the Gulf of Mexico, a land locked tropical basin in north-western Atlantic and on similar latitudinal bands as the NIO basins, also has a strong seasonal cycle in Δq and ΔT (Muller-Karger et al. 2015), but follows the global ocean patterns in LHF variability as seen in figure 1b, c. This suggests that merely having seasonality in Δq and ΔT is not enough to produce the kind of uniqueness in the wind and humidity control on LHF as seen in the NIO basins.

Figure 6 shows the seasonal cycle of ΔT, SST and T_a averaged over NAS, BoB and Gulf of Mexico. The seasonal amplitude of ΔT in NAS, BoB and Gulf of Mexico are ~1°C, ~1.4°C and ~2°C respectively, suggesting that Gulf of Mexico has the largest amplitude ΔT. Similarly the annual amplitude of SST and T_a in the Gulf of Mexico are also much larger than that in the NIO basins (see figure 6b). Then what makes the NIO basins so unique? A closer examination of ΔT in figure 6a suggests that the minimum in ΔT in the NIO basins, which is close to 0°C, coincides with higher values of SST and T_a (both higher than 28°C). At the same time, minimum in ΔT in Gulf of Mexico happens in March-April-May when the average SST and T_a are less than 24°C. In Gulf of Mexico, when SST reaches its peak climatological values of 29.5°C in JJA, ΔT is fairly large at ~1°C and is still increasing. Another important point to note is that, when SST is

higher than 25°C, T_a warms faster than SST in the NIO basins, whereas in the Gulf of Mexico, SST warms faster than T_a. This feature causes a number of differences in the dynamic and thermodynamic properties of the lower boundary layer as far as the turbulent flux exchanges are concerned. In NIO, when SST warms above the 25°C threshold, the T_a warms faster and closes the gap in the humidity gradient between sea and air, thus producing a negative feedback from the thermodynamic processes. In Gulf of Mexico, when SST warms above 25°C, SST warms faster than T_a, thus increasing the vertical humidity gradient and hence the LHF loss. Thus, although both NIO basins and Gulf of Mexico have strong seasonality in SST, T_a and ΔT, the differential rates of SST and T_a warming above the threshold temperature of 25°C, make the NIO basin behave differently compared to the Gulf of Mexico.

3.3. Dynamic and thermodynamic contributions on LHF variability as a function of SST

Figure 7 shows the climatology of SST, W_s and Δq (left panel) and the contributions from dynamic and thermodynamic processes on the total LHF variability with respect to SST (right panel). For this analysis, a daily climatology (365 days) is first calculated based on 1985-2013 daily data and then a 31 day running smoothing is applied to remove any high frequency variability. Figure 7a-c suggests that wind speed and Δq in NIO have a much stronger climatological annual cycle and SST a much strong semi-annual cycle than found in the west Pacific warm pool or the tropical ocean average. The climatological SST maxima and wind speed maxima in the NIO basins broadly coincide, and thus result in a positive correlation between the two (r=0.35 at 99% significance level). Thus according to the bulk formulae and the equation described in (2), this coincident SST and wind variability results in a net increase of LHF with increase in SST as shown in figure 7e. Similarly figure 7a and 7c suggest that SST and Δq have an anti-phase relationship. Thus this negative correlation (r=-0.5 at 99% significance level) results

in a thermodynamic feedback with a net decrease of LHF with increase in SST as shown in figure 7e.

In the tropical west Pacific (130-160°E,10°S-10°N) and generally over the whole tropics, annual cycle of SST, W_s and Δq are very weak. Also, SST and W_s (Δq) are in anti-phase (in-phase) relationship at annual timescales. Thus with an increase in SST, the Δq increases, leading to more LHF loss from ocean (figure 7f). At the same time, SST warming leads to convergence and weaker winds as described by Ramanathan and Collins (1992), and results in a reduction in LHF loss (figure 7e). These processes compensate each other and sometimes dominate over the other at certain seasons as seen in figure 7d. In the NIO basins, the net effect is such that latent heat flux is driven by the thermodynamic processes most of the seasons although this effect peaks in JJA.

4. Summary and Discussion

4.1 Summary

LHF both affects SST and is affected by SST. As LHF increases, SST decreases, unless countered by other processes. The dependency of LHF on SST changes is more complicated and has both a thermodynamic component in which SST affects the vertical humidity gradient, and a dynamic component in which SST affects the surface wind speed. Positive feedbacks can occur when a positive anomalous SST gives rise to a reduced LHF that reinforces the positive anomalous SST. The Wind-Evaporation-SST (WES) feedback of Xie and Philander (1994) is one such feedback. In contrast, if an increase in SST leads to an increase in LHF, then a negative feedback exists resulting in a stable SST value. Understanding these processes and feedbacks are important for understanding how an equilibrium SST is maintained. In this study, we attempt

to analyze the dynamic and thermodynamic feedback relations between LHF and SST in the global oceans, but particularly focusing on the tropical basins. Our analysis suggests that due to land effects on the air-sea interaction, northern tropical Indian Ocean comprising Bay of Bengal (BoB) and Northern Arabian Sea (NAS) is unique among the rest of the basins when considering the role of wind speed and vertical humidity gradient on latent heat flux. Hence much of our attention is drawn into the north Indian Ocean conditions.

In the global oceans, the contribution of surface wind speed and air-sea humidity gradient as functions of SST on the LHF variability are stronger and more pronounced in the tropical belt, especially over warm waters with SST more than 25°C. Generally, wind as a function of SST decreases the LHF upto a maximum rate of ~15W/m^2/°C in the tropical warm waters. This is because low pressure systems form over warm waters in the tropical belt that supports low level convergence and ascent of moist air. Surface winds are weaker over the convergence zones, and thus warm SST supports weaker winds, and hence a decrease in LHF. Likewise, over warm waters, the saturation humidity of the near surface increases, thus increasing the vertical humidity gradient. Hence increase in SST leads to an increase in vertical humidity gradient which then drives more LHF loss, upto a maximum rate of ~15W/m^2/°C in tropics. Thus in different basins, one of these two processes dominates over the other, and leads to either increase of LHF loss or decrease of it at different rates with SST (see figure 1a).

The two north Indian Ocean (NIO) basins, i.e., NAS BoB exhibit unique wind and humidity relationships with LHF, which are not consistent with the global ocean patterns. Unlike the global relationships, our analysis suggests that in the two NIO basins, there is a net increase (decrease) of LHF with respect to winds (vertical humidity gradient) with increase in SST at annual timescales. This uniqueness in the wind versus vertical humidity on LHF in the NIO

basins is attributed to the strong seasonality of the LHF controlling variables (wind and vertical humidity gradients) and also to the large seasonality in the air-sea temperature gradients maintained by the large scale, monsoon dominated wind patterns. Large scale upper air circulation pattern over the BoB and NAS is such that it is always of land origin irrespective of its seasonal reversal in direction, which has large consequences on the LHF variability in the ocean. During summer (winter), the upper air circulation brings in warm (cold) and dry air from the land into the BoB and NAS basins, thus making the lower layers of the boundary layer warm (cold). This warm (cold) air advection from the land warms (cools) the air column over the NIO basins faster than elsewhere in the global oceans. This helps in maintaining a small (large) air-sea temperature gradient over BoB and NAS during summer (winter). In rest of the basins, the Δq and ΔT are maintained fairly constant throughout.

We have further shown that, having strong seasonality in ΔT (and hence in Δq) is not a lone condition for the unique features seen in the NIO basins. Gulf of Mexico, another tropical basin in comparable latitudinal bands, also exhibits strong seasonal cycles in ΔT and Δq, but does not show the kind of wind and humidity effects on LHF as seen in NIO. Firstly, in NIO basins, the minimum in ΔT (and Δq) is observed when SST and T_a are warmer (>28°C).Whereas in Gulf of Mexico, the minimum in ΔT is seen when SST and Ta are still cold (<25°C). This difference is due to the stronger influence of land heating of the air that is advected over the NIO basins. As a consequence, the normally warm basins like the BoB and NAS are more reactive to air-sea coupling compared to Gulf of Mexico. Secondly, in the NIO basins, over warm waters of SST>25°C, T_a warms faster than SST, thus bringing down the air-sea temperature and humidity gradient. Hence in the NIO basins, for any increase in SST, the Δq affects a decrease in LHF. Whereas in Gulf of Mexico, over warm waters of SST>25°C, SST warms faster than T_a, thus

increasing the air-sea temperature and humidity gradient. This differential warming of SST and T_a in the NIO basins and Gulf of Mexico are the reasons for the differences in the contribution of wind and vertical humidity gradients as functions of SST on LHF as seen in figure 1.

4.2 Discussion

Our results are in general agreement with ZM95 results from the tropical Pacific. A closer examination of our results from figure 3 suggests that humidity gradient increases with SST in most of the seasons in NIO, consistent with the relationships described in ZM95 (their figure 8). Wind variations with respect to SST are also similar (compare our figures 3c,d with ZM95 figure 7). But the very large seasonal range of the NIO basins means that the annual average profile of Δq and W_s look differently than that of the tropical Pacific.

ZM95 and Nisha et al (2014) looked to find a threshold SST where the roles of wind speed and humidity gradient reverses its influence on LHF. Our intent is to expand this type of analysis to the global oceans, while maintaining a focus on the tropics and the NIO in particular. One major drawback of our methodology is that other processes besides LHF can also affect SST variations. For example, the LHF will affect the hydrological cycle and cloud formations, which can then affect the solar and longwave radiation that is absorbed by the ocean surface. Similarly, wind variations, in addition to affecting LHF, can affect upper ocean turbulence and ocean currents, which can then affect SST through mixing and advection. To the extent that these processes are correlated, they may be entering the LHF-SST feedbacks observed here. We have attempted to distinguish ocean-driven variations from land affects by comparing the amplitudes of sea surface vs. surface air temperature variations. We show that land clearly influences the LHF – SST feedbacks in the NIO basins. Analysis of a coupled model could help better understand these feedbacks. Our analysis further suggests that errors in the proper

simulation of the dynamic and thermodynamic components of LHF can have strong impact on SST biases in the forecasting models, which needs further detailed analysis.

Many studies report of a warming ocean (Levitus et al. 2000). In a warming scenario in the NIO basins, it can be speculated that the surface air over the oceans might warm faster (as shown in this paper) and become more saturated leading to decrease the LHF loss. This can become a reinforcing mechanism for further SST warming (unless it is compensated by increased LHF loss by strengthened winds). This scenario, in which thermodynamic negative feedback dominates, is possible if the advecting air from the continent brings more heat over the ocean. But if the opposite happens, i.e., if SST warms and T_a does not warm as fast as that of SST, the LHF-SST relation can become a damping mechanism for the SST warming. All these scenarios have corresponding changes in the wind speed and cloudiness that are not well understood. In a global warming perspective, these possibilities need further detailed analysis using long term observations and coupled model analyses.

Acknowledgements

The authors are grateful to the Editor and three anonymous reviewers for their time and constructive comments, which helped us to improve an earlier version of the manuscript. We thank the Director, Indian National Centre for Ocean Information Services (INCOIS), for the encouragement and Ministry of Earth Sciences (MoES), Govt. of India for financial support. We also thank OAFlux, and NCEP-NCAR projects for providing the datasets. Discussions with Jerome Vialard (LOCEAN/IRD, Paris) helped to improve the article. This is INCOIS contribution number 265 and PMEL contribution number 4463.

Appendix

Land Influence on the air temperatures of the North Indian Ocean Basins

Since land effect on the T_a over the two NIO basins is a key point of this article, here we provide a further discussion on the same. As discussed in Section 3.2, the NAS and BoB T_a patterns are influenced by monsoon reversal of winds. Figure A1 provide a zoomed in version of the T_a (colors) and 1000mb to 850 mb averaged wind patterns over the NIO basins averaged over September through February (figure A1a) and March through August (figure A1b).

During September through February, the mean wind patterns over the NIO basins is north-easterly (figure A1.a). The north-eastern part of the AS experience an advection of cold air from Pakistan-Iran land mass, which is colder than that over AS. Whereas the eastern portion of the Arabian Sea experience an advection of air from central India and is comparatively warmer than that blowing from Pakistan-Iran into the north-east of Arabian Sea. This limits the cold air effects in the north-west of AS and that region becomes colder compared to other regions of AS. During pre-monsoon and monsoon seasons (March through August), Indian subcontinent and Arabian Peninsula are the warmest regions in the entire tropical basins (figure A1.b; also refer figure 5). There is a component of wind coming from Pakistan-Iran and another one parallel to the Persian Gulf, which discharge very warm air mass into the northern AS. The geographic location of AS and the mean wind directions are such that the influence of hot air that blows from land to AS are limited to the north-western AS (Bhat and Fernando. 2016).

In the BoB, during September through February, the mean wind pattern is north-easterly which brings in very cold air from the Himalayan footprints (figure A1.a) into the Bay thus substantially decreasing T_a there. From March through August, the south-west monsoon winds over the Bay are coming from the much warmer Indian subcontinent, and hence increases the T_a over the Bay.

Thus in both basins, from September through February, cold air comes from the nearest land mass, and reduces the T_a over the oceans. During the rest of the time, the warm air coming from the land increases the T_a over the oceans. The only difference between the air circulation patterns between NAS and BoB is that in NAS land influence always comes from north-west of the AS and limited to north-west AS whereas in Bay of Bengal during winter it comes from north (Himalayan foothills) and in summer it comes from west (Indian subcontinent), and influences entire Bay.

References

Alexander, M. A. and Scott, J. D., 1997: Surface flux variability over the North Pacific and North Atlantic Oceans. J. Climate, **10**. pp. 2963-2978.

Barsugli, J. J., and D. S. Battisti, 1998: The basic effects of atmosphere-ocean thermal coupling on mid-latitude variability, *J. Atmos. Sci*., **55**, 477–493.

Bhat, G.S., and H.J.S. Fernando. 2016. Remotely driven anomalous sea-air heat flux over the north Indian Ocean during the summer monsoon season. *Oceanography* 29(2):232–241, http://dx.doi.org/10.5670/oceanog.2016.55.

Bhat, G. S., S. Gadgil, P. V, Harish Kumar, S. R. Kalsi, Madhusoodanan, V. S. N. Murty, C. V. K. PrasadaRao, V. Ramesh Babu, L. V. G. Rao, R. R. Rao, M. Ravichandran, K. G. Reddy, P. SanjeevaRao, D. Sengupta, D. R. Sikka, J. Swain, P. N. Vinayachandran, 2001: BOBMEX - the Bay of Bengal Monsoon Experiment. *Bull. Amer. Meteor. Soc*., **82**, 2217-2243.

Bhat, G. S., 2001: Near surface atmospheric characteristics over the North Bay of Bengal during the Indian summer Monsoon. *Geophys. Res. Lett*., **28**, 987-990.

de Boyer Montegut, C., Vialard. J, Shenoi. S. S. C, Shankar. D, Durand. F, Ethé. C, Madec. G, 2007: Simulated seasonal and interannual variability of mixed layer heat budget in the northern Indian Ocean, *J. Clim*, **20**, 3249–3268.

DiNezio, P. N., A. C. Clement, G. A. Vecchi, B. J. Soden, B. P. Kirtman and S.-K. Lee, 2009: Climate response of the equatorial Pacific to global warming. J. Clim, **22**, 4873-4892

Fairall., C. W., Bradley. E. F, Hare. J. E, Grachev. A. A, Edson. J. B, 2003: Bulk parameterization on air-sea fluxes: updates and verification for the COARE algorithm. *J Clim*,**16**:571–591

Fairall., C. W., Bradley. E. F, Rogers. D. P, Edson. J. B, Young. G. S, 1996: Bulk parameterization of air-sea fluxes for tropical ocean-global atmosphere coupled ocean-atmosphere response experiment. *J Geophys Res***101**:3747–3764

Frankignoul., C , and K. Hasselmann, 1977: Stochastic climate models. Part 2. Application to sea-surface temperature variability and thermocline variability.*Tellus*, **29**, 284–305.

Gao, S., L. S. Chiu, and C.-L. Shie, 2013: Trends and variations of ocean surface latent heat flux: Results from GSSTF2c data set. Geophys. Res. Lett., 40, 380–385, doi:10.1029/2012GL054620

Kalnay., E et al (1996) The NCEP/NCAR 40-year reanalysis project. *Bull Am Meteor Soc***77**:437–470

Levitus, S., J. I. Antonov, T. P. Boyer, and C. Stephens, 2000: Warming of the world ocean. *Science*, **287**, 2225–2229.

Liu., W. T, 1988: Moisture and latent heat flux variabilities in the tropical Pacific derived from satellite data. *J. Geophys. Res*., **93**, pp. 6749-6760.

Muller-Karger., F. E, J.P. Smith, S. Werner, R. Chen, M. Roffer, Y. Liu, B. Muhling, D. Lindo-Atichati, J. Lamkin, S. Cerdeira-Estrada, D.B. Enfield, 2015: Natural Variability of Surface Oceanographic Conditions in the Offshore Gulf of Mexico, *Prog. Oceanogr*. **134**, 54-76

Neelin., J. D, and I. M. Held, 1987: Modeling tropical convergence based on the moist static energy budget. *Mon. Wea. Rev*., **115**, pp. 3-12.

Nisha., P. G., Muraleedharan, P. M, Keerthi. M. G, Sathe. P. V and Ravichandran. M, 2012: Does sea level pressure modulate the dynamic and thermodynamic forcing in the tropical Indian Ocean? *International Journal of Remote Sensing*, **33 (7),** pp. 1991-2002

Ramanathan., V and W. Collins, 1992: Thermostat and global warming. Nature, **357**, 649.

Schott., F. A., S. -P. Xie and J. P. McCreary Jr., 2009: Indian Ocean circulation and climate variability. *Rev. Geophys.,***47**, RG1002, doi:10.1029/2007RG000245

Seager., R., R. Murtugudde, A. Clement, and C. Herweijer, 2003: Why is there an evaporation minimum at the equator? *J. Climate*, **16**, 3793–3802.

Sengupta, D., S. R. Parampil, G. S. Bhat, V. S. N. Murty, V. Ramesh Babu, T. Sudhakar, K. Premkumar, and Y. Pradhan, 2008: Warm pool thermodynamics from the Arabian Sea Monsoon Experiment (ARMEX), *J. Geophys. Res.*, **113**, C10008, doi:10.1029/2007JC004623.

Sobel, A. H., 2003: On the coexistence of an evaporation minimum and precipitation maximum in the warm pool. *J. Clim*, **16**, 1003–1009.

Sui., C. -H, K, M. Lau and A. K. Betts, 1991: An equilibrium model for the coupled ocean-atmosphere boundary layer in the tropics. *J. Geophys. Res*., **96**, pp. 3151-3163.

Wallace., J. M., 1992: Effect of deep convection on the regulation of tropical sea surface temperature, *Nature*, **357**, 230 – 231.

Wu., R, Kirtman. B. P, Pegion. K, 2007: Surface latent heat flux and its relationship with sea surface temperature in the national centers for environmental prediction climate forecast system simulations and retrospective forecasts. *Geophys Res Lett* 34:L17712.doi:10.1029/2007GL030751

Wu., R., B. P. Kirtman, and K. Pegion, 2006: Local air-sea relationship in observations and model simulations, *J. Clim*., **19**, 4914 – 4932.

Xie, S.-P., and S. G. H. Philander, 1994: A coupled ocean-atmosphere model of relevance to the ITCZ in the eastern Pacific, Tellus, Ser. A, 46, 340-350.

Yu., L, Jin. X, Weller. R. A, 2007: Annual, seasonal, and interannual variability of air sea heat fluxes in the Indian Ocean. *J Clim***20**:3190–3209

Zhang, G.J. and M.J. McPhaden, 1995: On the relationship between sea surface temperature and latent heat flux in the equatorial Pacific. *J. Climate, **8***, 589-605.

Zhang, G.J., V. Ramanathan, and M.J. McPhaden, 1995: Convection-evaporation feedback in the equatorial Pacific. *J. Climate,* **8**, 3040-3051.

Figure captions

Figure 1: (a) Variation of Latent Heat Flux (LHF) with respect to unit change of Sea Surface Temperature (SST), (b) thermodynamic contribution of humidity gradient variation associated with unit SST change on LHF change and (c) dynamic contribution of wind speed variation associated with unit SST change on LHF change. Mean SST contours for 25°C and 28°C are marked in the three panels. Unit of shaded values is $W/m^2/°C$. Boxes indicate the Bay of Bengal

and North Arabian Sea. This calculation was done using daily OAFlux data from 1985 to 2013 and is significant at 99% confidence level.

Figure 2: Binning analysis of (a) humidity gradient, (b) wind speed and (c) latent heat flux as functions of SST in North Arabian Sea ([60-72°E,16-25°N]), Bay of Bengal ([80-95°E,10-24°N]) and Global Tropical Oceans ([0-360°E, 30°S-30°N]) using OAFlux data. The bin size selected is 1°C on the x-axis. Shading shows 1 standard deviation and the vertical lines show SST bound of 25°C to 28°C. For clarity, shading is not shown for the global tropics.

Figure 3: Binning analysis of (a, b) humidity gradient, (c, d) wind speed and (e, f) latent heat flux as functions of SST in North Arabian Sea ([60-72°E,16-25°N], left column) and Bay of Bengal ([80-95°E,10-24°N]; right column) for different seasons using OAFlux data. The bin size selected is 1°C on the x-axis. Shading shows 1 standard deviation and the vertical lines show SST bound of 25°C to 28°C. For clarity, shading is only shown for the annual case.

Figure 4: Time mean of (a) Sea – Air temperature gradient (SST – air temperature at 2m height), (b) rate of change of temperature gradient with respect to SST and (c) moisture holding capacity of 2m air estimated following Magnus formula, for SST in the range 25°C<SST<28°C. The boxes indicate the Bay of Bengal and North Arabian Sea. Statistical significance of the regression analysis is done for figure 4b and those not significant at 99% confidence level are masked from the three panels.

Figure 5: Climatological surface air temperature averaged over 1000mb to 850mb (colors) and surface wind vectors (arrows) over the tropical oceans for (a) DJF (b) MAM (c) JJA and (d) SON periods from NCEP

Figure 6: Climatology of (a) sea-air temperature gradient and (b) SST (full line) and air temperature (dotted line) in Bay of Bengal , North Arabian Sea and Gulf of Mexico from OAFlux data.

Figure 7: Annual cycles of (a) Sea Surface Temperature, (b) wind speed (c) humidity gradient, (d) LHF variation as a function of SST, (f) wind contribution into the LHF variability and (e) humidity gradient contribution into the LHF variability using OAFlux data. Different basins are marked with different line styles as shown in figure 7c.

Figure A1. Climatological surface air temperature and surface wind vectors (arrows) averaged over 1000mb to 850mb (colors) over the North Indian Ocean for (a) DJFMAM and (b) JJASON periods. Boxes are drawn to highlight the land origin of air advecting into the NIO basins.

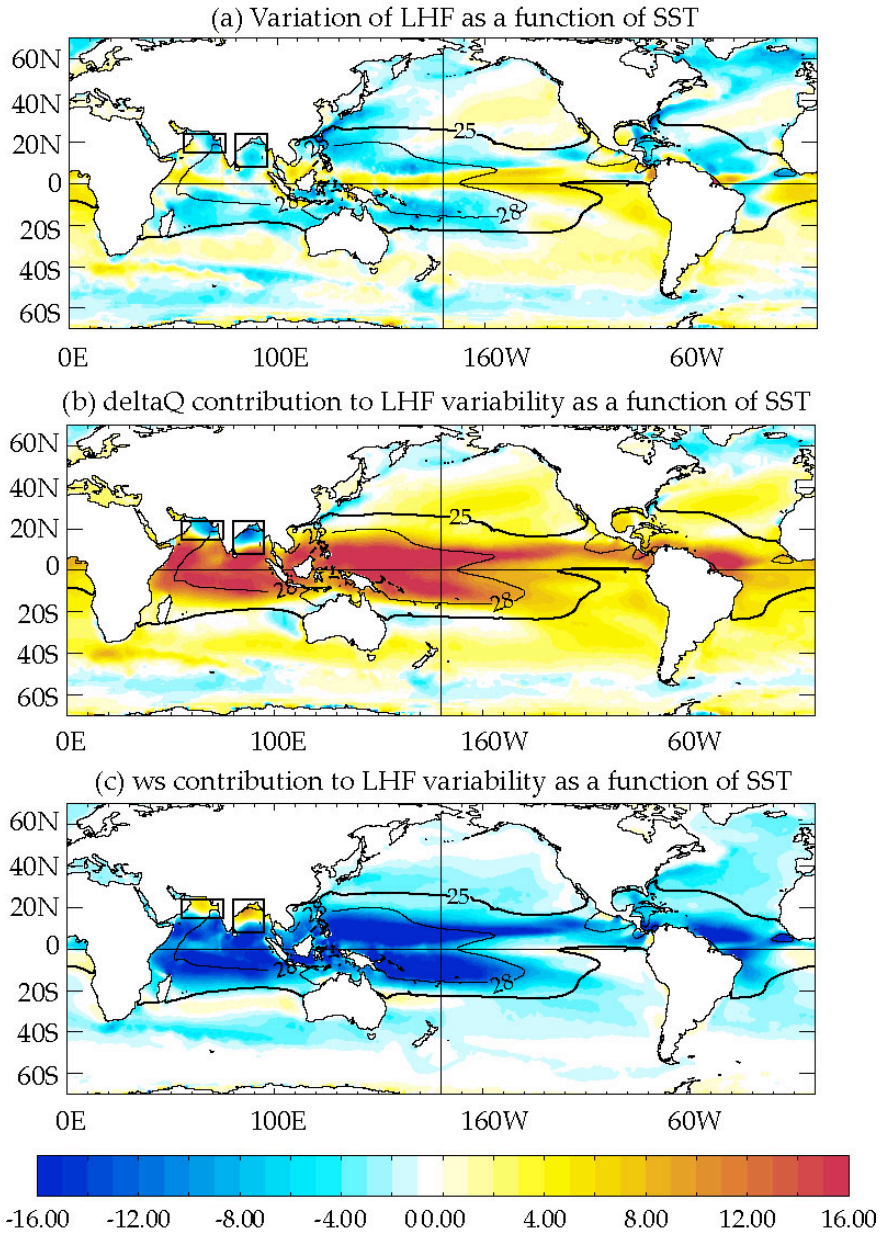

Figure 1: (a) Variation of Latent Heat Flux (LHF) with respect to unit change of Sea Surface Temperature (SST), (b) thermodynamic contribution of humidity gradient variation associated with unit SST change on LHF change and (c) dynamic contribution of wind speed variation associated with unit SST change on LHF change. Mean SST contours for 25°C and 28°C are marked in the three panels. Unit of shaded values is $W/m^2/°C$. Boxes indicate the Bay of Bengal

and North Arabian Sea. This calculation was done using daily OAFlux data from 1985 to 2013 and is significant at 99% confidence level.

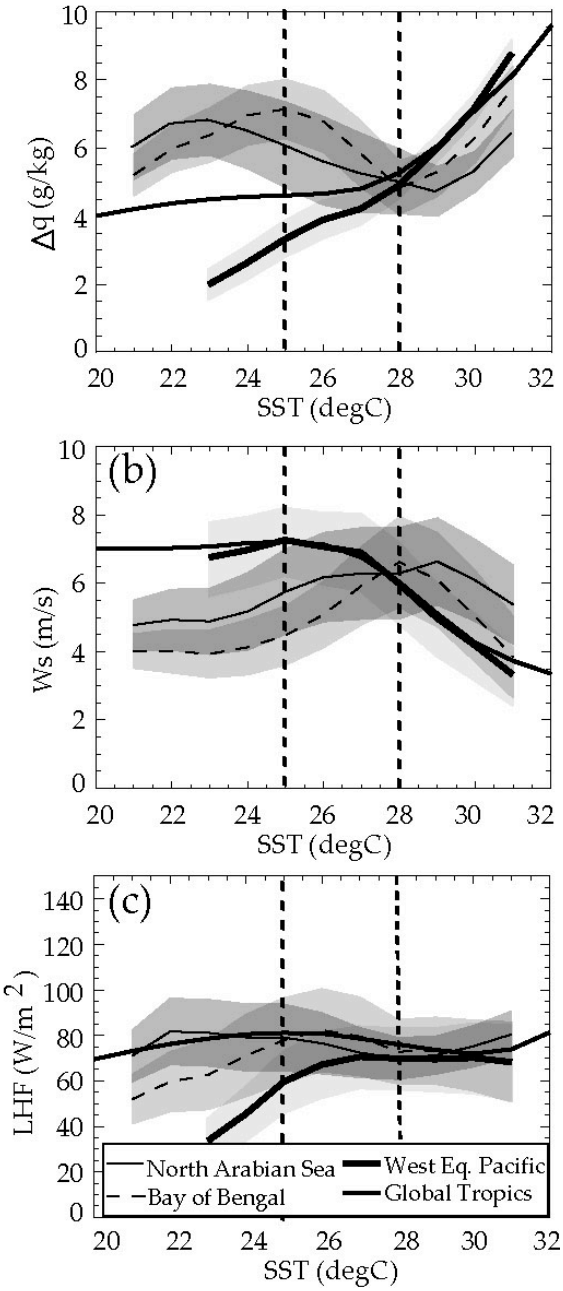

Figure 2: Binning analysis of (a) humidity gradient, (b) wind speed and (c) latent heat flux as functions of SST in North Arabian Sea ([60-72°E,16-25°N]), Bay of Bengal ([80-95°E,10-24°N]), western equatorial Pacific ([130-160°E,10°S-10°N]) and Global Tropical Oceans ([0-

360°E, 30°S-30°N]) using OAFlux data. The bin size selected is 1°C on the x-axis. Shading shows 1 standard deviation and the vertical lines show SST bound of 25°C to 28°C. For clarity, shading is not shown for the global tropics.

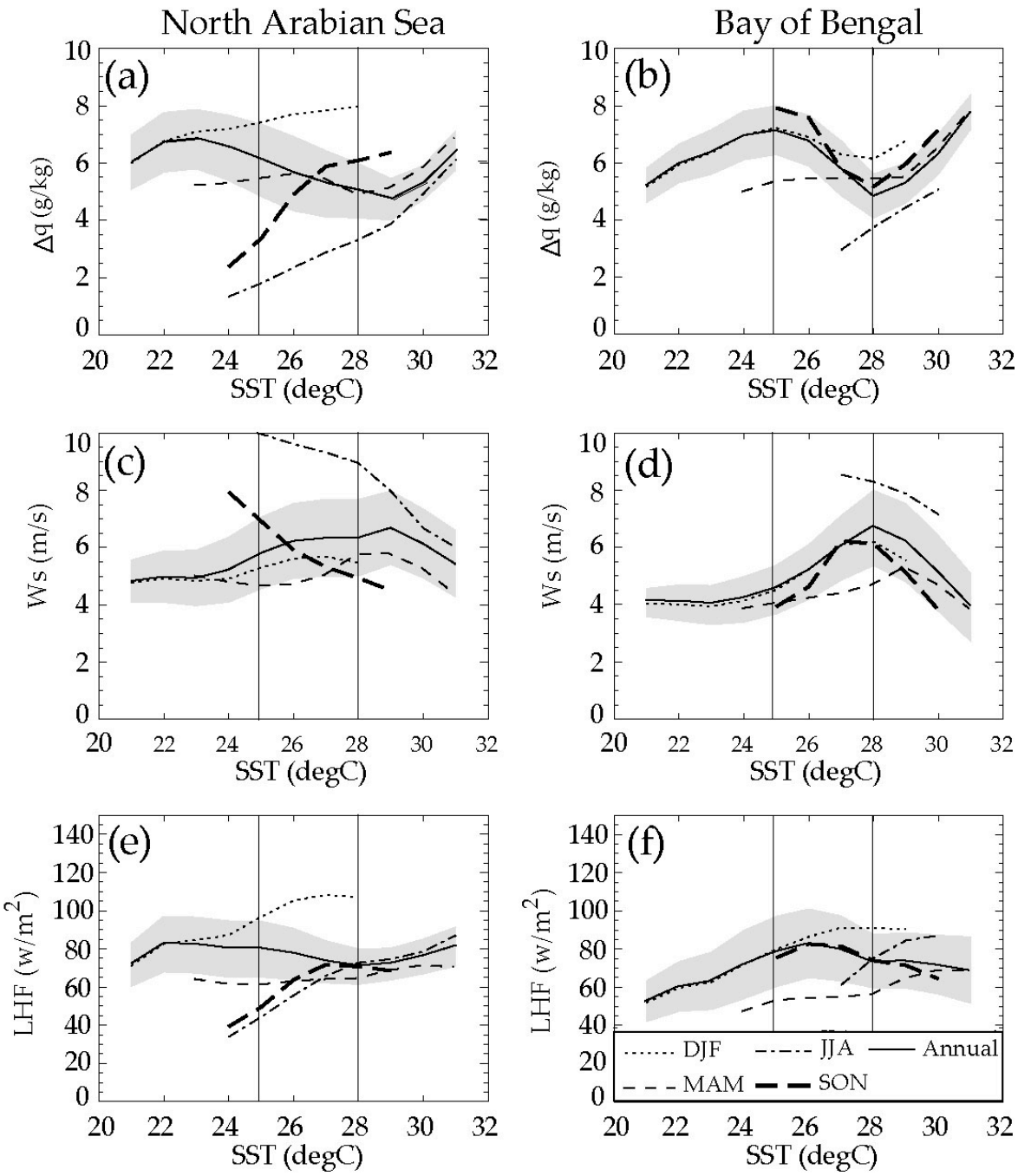

Figure 3: Binning analysis of (a, b) humidity gradient, (c, d) wind speed and (e, f) latent heat flux as functions of SST in North Arabian Sea ([60-72°E,16-25°N], left column) and Bay of Bengal ([80-95°E,10-24°N]; right column) for different seasons using OAFlux data. The bin size selected is 1°C on the x-axis. Shading shows 1 standard deviation and the vertical lines show SST bound of 25°C to 28°C. For clarity, shading is only shown for the annual case.

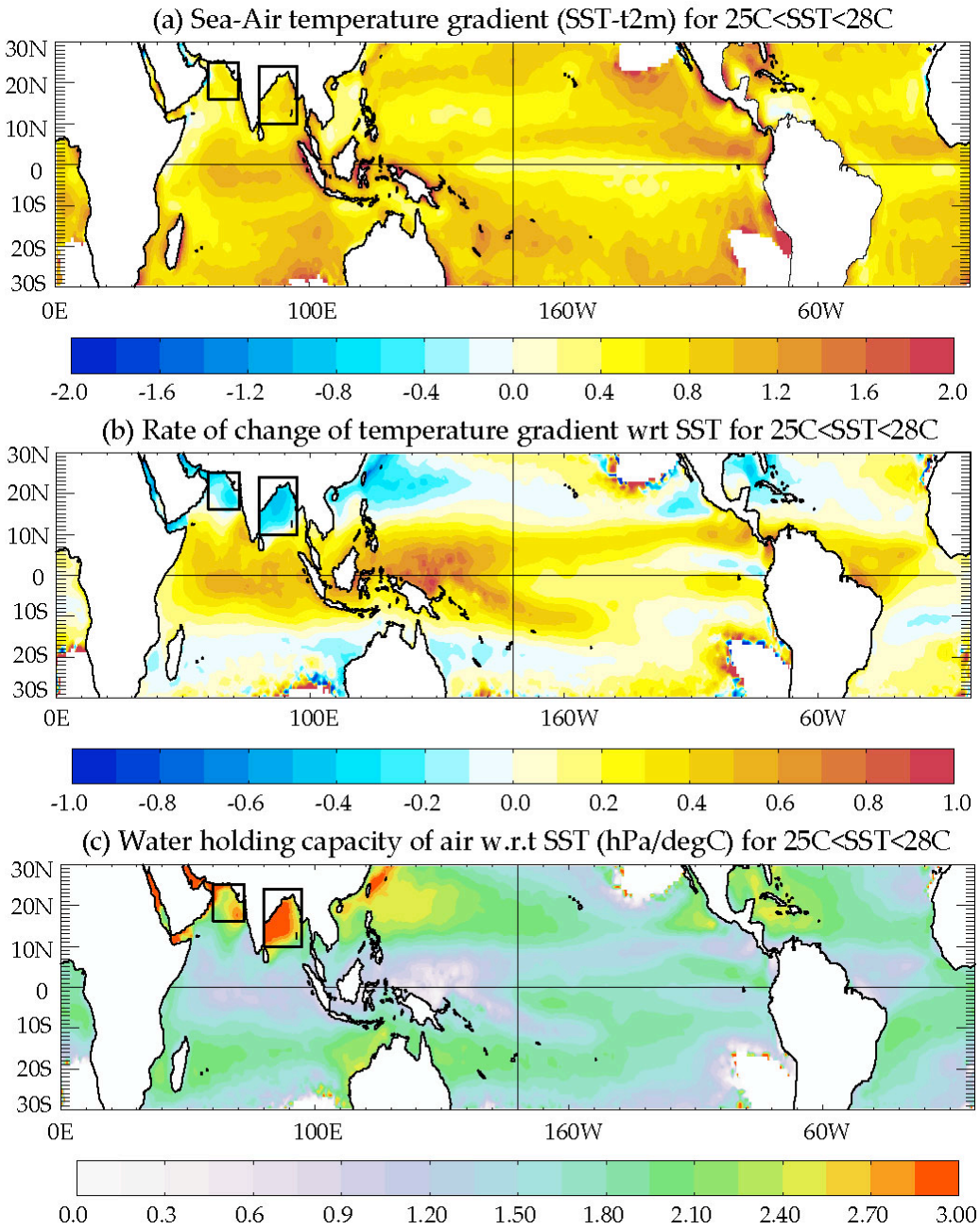

Figure 4: Time mean of (a) Sea – Air temperature gradient (SST – air temperature at 2m height), (b) rate of change of temperature gradient with respect to SST and (c) moisture holding capacity of 2m air estimated following Magnus formula, for SST in the range 25°C<SST<28°C. The boxes indicate the Bay of Bengal and North Arabian Sea. Calculations are done using OAFlux variables with different lengths of data at each grid point. Statistical significance of the

regression analysis is done for figure 4b and those not significant at 99% confidence level are masked from the three panels.

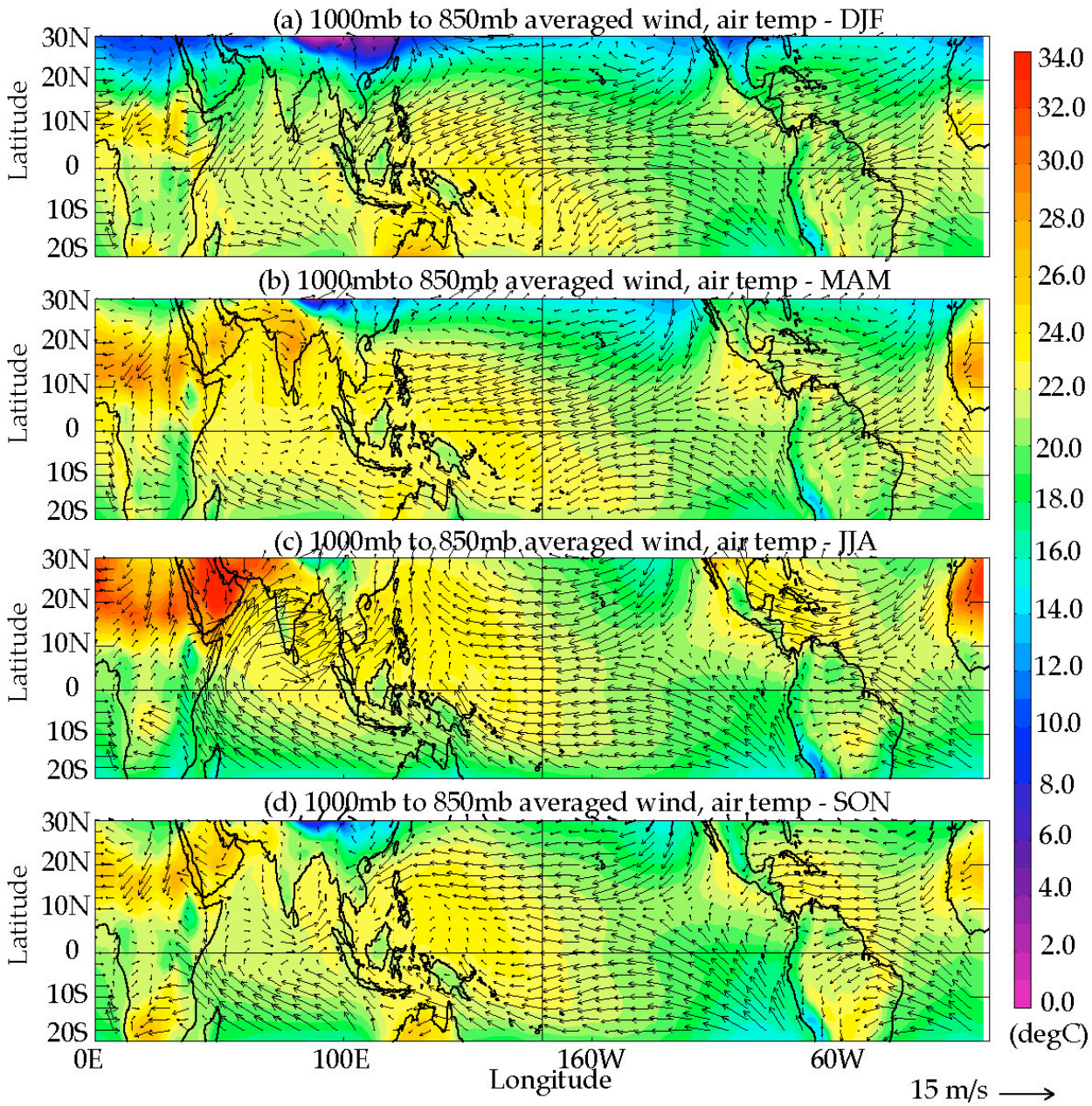

Figure 5: Climatological surface air temperature averaged over 1000mb to 850mb (colors) and surface wind vectors (arrows) over the tropical oceans for (a) DJF (b) MAM (c) JJA and (d) SON periods from NCEP

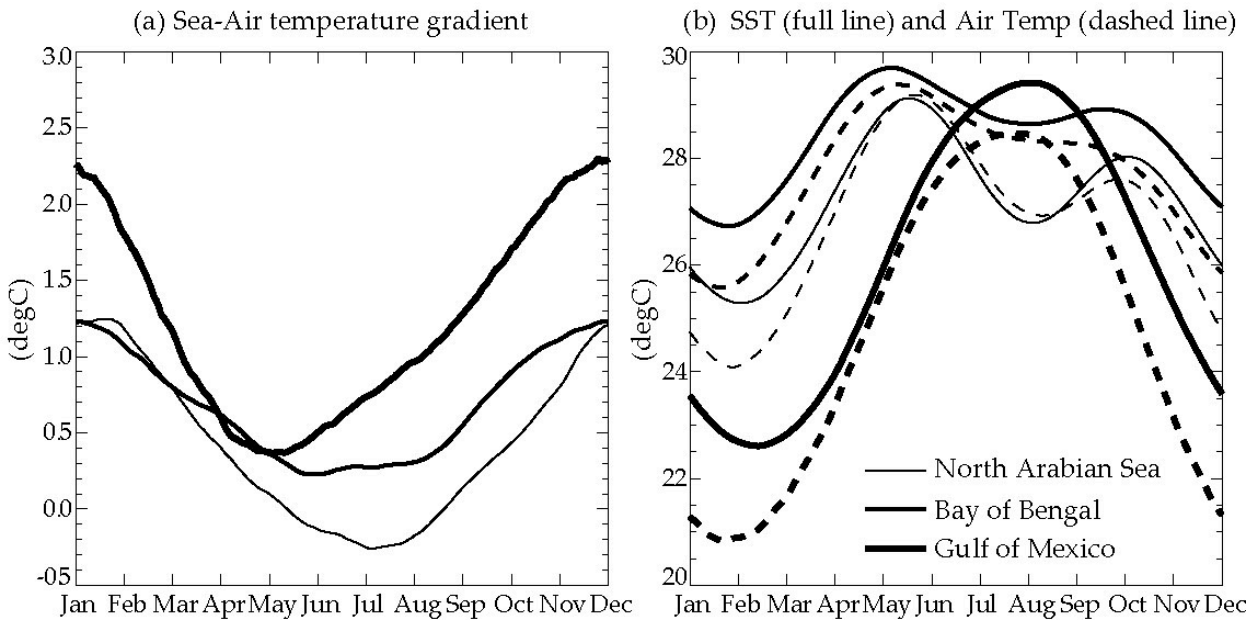

Figure 6: Climatology of (a) sea-air temperature gradient and (b) SST (full line) and air temperature (dotted line) in Bay of Bengal , North Arabian Sea and Gulf of Mexico from OAFlux data.

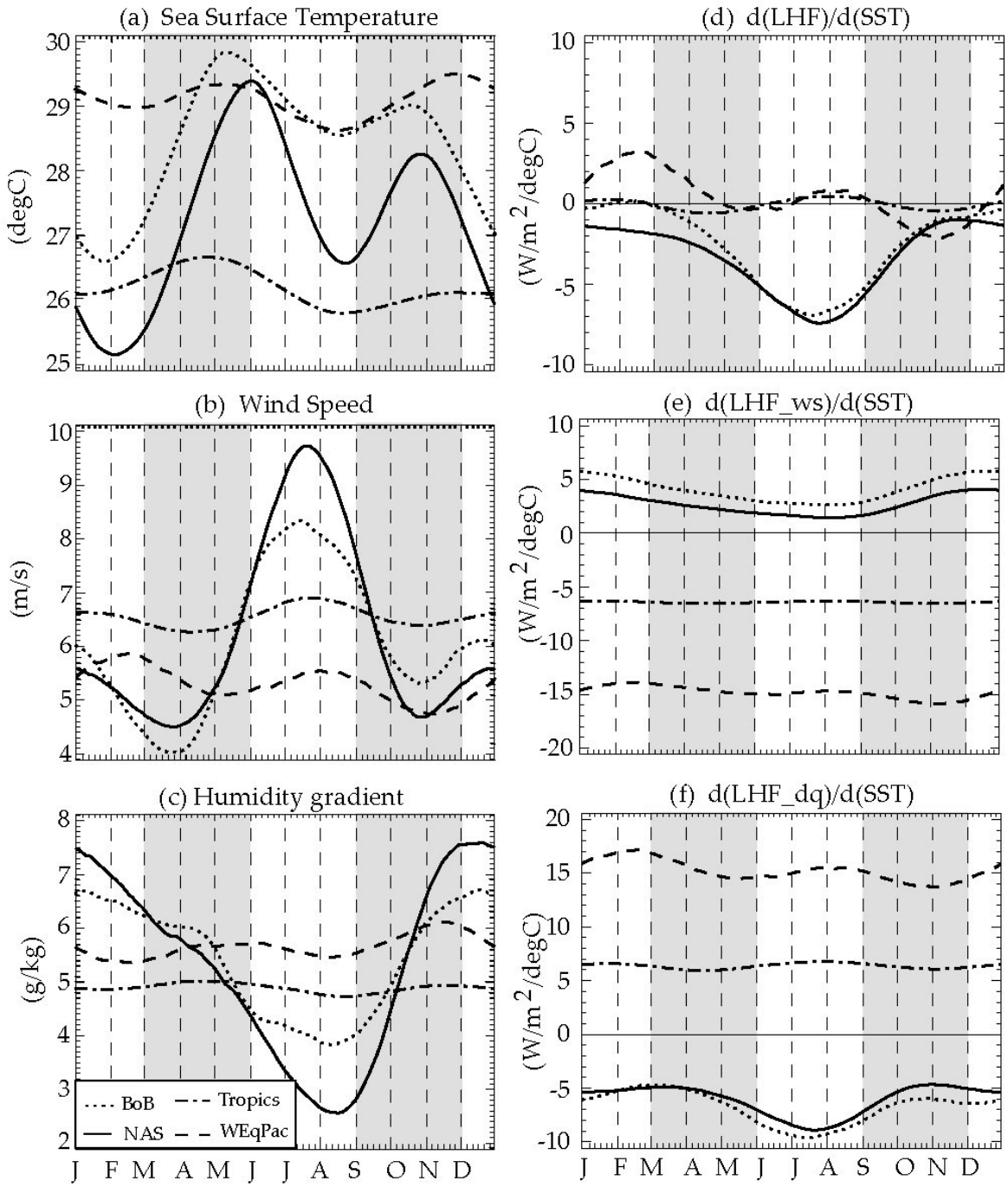

Figure 7: Annual cycles of (a) Sea Surface Temperature, (b) wind speed (c) humidity gradient, (d) LHF variation as a function of SST, (f) wind contribution into the LHF variability and (e) humidity gradient contribution into the LHF variability using OAFlux data. Different basins are marked with different line styles as shown in figure 7c.

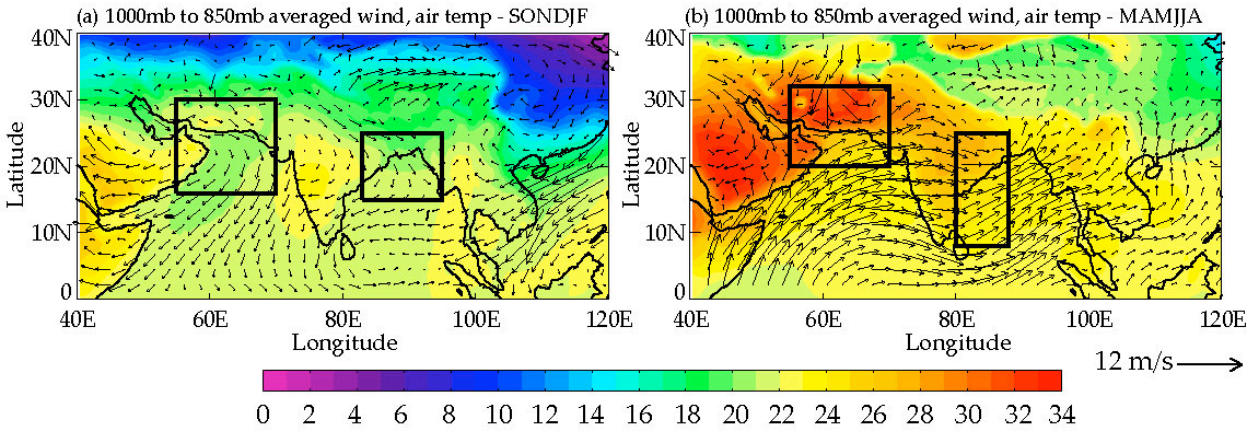

Figure A1. Climatological surface air temperature and surface wind vectors (arrows) averaged over 1000mb to 850mb (colors) over the North Indian Ocean for (a) DJFMAM and (b) JJASON periods. Boxes are drawn to highlight the land origin of air advecting into the NIO basins.